A Novel and More Efficient Way to Grind Punching Tools

P. Krajnik[1,2], R. Drazumeric[2], J. A. Badger[3], C. M. Nicolescu[1], J. Kopac[2]
[1]KTH Royal Institute of Technology, Production Engineering, Stockholm, Sweden
[2]University of Ljubljana, Faculty of Mechanical Engineering, Ljubljana, Slovenia
[3]The Grinding Doc Consulting, Austin, Texas, USA
peter.krajnik@iip.kth.se

ABSTRACT

A simulation model of punch grinding has been developed which calculates the instantaneous material-removal rate, arc length of contact and temperature based on the kinematic relationships between wheel and workiece and determines the optimum machine parameters to reduce cycle time and achieve a constant-temperature no-burn situation. Two basic outputs of the simulation model include arc length of contact and specific material-removal rate. A thermal model is included in the simulation to calculate maximum grinding zone temperature rise. A novel method is developed to constrain this temperature rise in the simulation. The thermal model inputs a constant value of specific grinding energy and the energy partition, which represents the fraction of the grinding energy conducted as heat to the workpiece. The simulation-based optimization can lead to a drastic reduction of grinding cycle time. Moreover, the limitation of maximum grinding zone temperature rise below the transitional temperature can help to avoid generation of workpiece thermal damage, which includes thermal softening, residual tensile stress, and rehardening burn. The grindability of high speed steel (HSS) is also discussed in terms of power consumption, specific grinding energy and undeformed chip thickness.

Keywords: Grinding, Modeling, Simulation, Geometry, Thermal.

1. INTRODUCTION

AISI M2 (EN HS6-5-2) HSS for cold work applications is widely used for production of punching tools due to its high thermal stability combined with high hardness and wear resistance. These properties make HSS more difficult to grind than other steels, especially when using conventional aluminium-oxide wheels. The grindability is largely affected by the hard tungsten-molybdenum- and vanadium-carbides held firmly in the hardened-steel matrix. High temperatures which can occur during grinding of HSS lead to various types of thermal damage, such as surface oxidation, softening, rehardening, residual stresses, and cracks [1].

Tensile residual stress is particularly critical because it reduces service life and reliability of an operating punching tool under fatigue conditions. Low tensile residual stress is therefore a key surface integrity requirement. The fatigue properties of punching tools are determined not only by the HSS material properties (e.g. carbide and inclusion contents, phase transformations) [2] but also by the thermophysical properties of the grinding process (chip thickness, wheel topography, energy partition, etc.), which affect the grinding temperatures. It was found that thermal stresses generated in the grinding process are the primary source of tensile residual stresses [3]. In this consideration, the problem of controlling residual stress is reduced into a problem of controlling grinding temperature.

For thermal analysis of grinding, it is of major importance to understand the factors which affect the grinding temperatures. An analytical temperature model is used in the simulation to avoid generating tensile residual stress. The model inputs the values of grinding geometry, kinematics and specific grinding energy. Another major factor for prediction of grinding temperatures is the energy partition, which represents the fraction of the grinding energy transported as heat to the workpiece.

Punch grinding is a special type of outside-diameter plunge grinding, performed on a cylindrical grinder. In order to grind a non-round profile on a punching tool, the radial infeed velocity (X-axis) must be synchronized with the workpiece velocity (C-axis) in a controlled manner. Improving the efficiency of punch grinding requires an optimization of grinding geometry and kinematics, which is based on a process simulation. The overall optimization objective, however, is to minimize grinding cycle time subject to constraint on maximum grinding zone temperature rise.

Early, and to our knowledge the only research on punch grinding included a development of the process simulation [4]. The developed simulation was used to predict material removal rate, arc length of contact, and the workpiece velocity. The major conclusions of this early research are summarized below [5]:

- Punch grinding at constant workpiece velocity leads to low material removal for most of the grinding cycle.

- Grinding cycle time can be reduced by increasing the workpiece velocity around the punch corner.

- The arc length of contact is over three times that of an equivalent sized round part in cylindrical grinding, leading to an increased threshold for the onset of thermal damage.

- The increased material-removal rate is best achieved by an increase in the workpiece velocity rather than by an increase in the depth of cut.

2. GRINDABILITY

It is well known that, within a family of HSS, different grades may have vastly different grindabilities, resulting in larger specific grinding energies and higher wheel wear (lower G-ratios) [6]. In HSS, tungsten-molybdenum- and, in particular, vanadium-carbides cause rapid dulling of Al_2O_3 grains. Figure 1 shows specific grinding energy (measured via grinding power) vs. the amount of material removed (measured as the volume of material removed per mm wheel width per mm wheel circumference) for grinding of different grades of HSS [7].

Experiments were carried out on a surface grinder using a 100%-white-Al_2O_3, 46-grit, H-grade, vitrified-bonded grinding wheel (diameter 350 mm, wheel speed 25 m/s), with 6% soluble oil grinding fluid and a cluster-diamond dresser (depth of dressing 25 μm and dressing lead of 0.2 mm/rev).
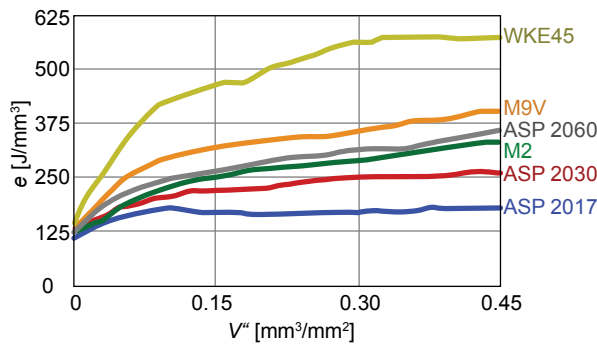

Fig. 1: Specific grinding energy vs. amount of material removed for six different HSS grades.

From the upper figure, we see that all grades begin at a specific grinding energy of around 125 J/mm^3. However, as some grades contain more and larger hard carbides, the specific grinding energies can increase drastically as grinding proceeds, resulting in one grade generating values of grinding power several times greater than grades with high grindability. Since temperature increase is directly proportional to grinding power, this results in much higher grinding temperatures.

3. SPECIFIC GRINDING ENERGY AND UNDEFORMED CHIP THICKNESS

Specific grinding energy e provides a valuable measure of the ability of a grinding wheel to remove material. Specific grinding energy depends on numerous factors, such as sharpness of the grinding wheel, the grindability of the workpiece material, undeformed chip thickness, cooling and lubrication, etc. There are several ways to calculate the undeformed chip thickness, h_m, depending on the shape of the undeformed chip volume. For the calculation of undeformed chip thickness we adopted the continuity analysis [6]. For the need of a simulation, h_m is expressed in terms of specific material removal rate Q'_w and arc length of contact l_c:

$$h_m = \sqrt{\frac{6}{C \cdot r} \frac{Q'_w}{v_s \cdot l_c}} \qquad (1)$$

where C is the cutting-point density, r is the shape factor, and v_s is the wheel velocity. Q'_w and l_c are constant in cylindrical grinding. In contrast, both parameters vary considerably within a single workpiece rotation when punch grinding, as shown later in Figure 6 and Figure 7.

Depending on the method, different values of shape factor can be used [8]. Here, a value of $r = 10$ was chosen. The cutting-point density, C, depends on the grit diameter and the dressing conditions and can change as the wheel wears. One simple method to calculate this value is [6]:

$$C = \frac{C_1}{d_g^{n_1}} \qquad (2)$$

where d_g is the grain diameter and C_1 and n_1 are constants. Numerous values of C_1 and n_1 have been found [6] depending on the bond type, dressing and also on the method of measurement. Here, values of $C_1 = 2$ and $n_1 = 1$ were chosen, which correspond to results found by Shaw [9].

Although different methods can be used to calculate h_m, we are most interested in relative values, which means the constants chosen above are adequate provided they are consistent throughout. Therefore, we can pluck various values of specific grinding energy from the already conducted experimental work [10] and power measurements made at various tool manufacturers grinding HSS with vitrified- and resin-bonded Al_2O_3 wheels. In all experiments oil was used as a grinding fluid. The power measurements were taken before the amount of material removed V_w" exceeded 0.1 mm^3/m^2. Figure 2 includes measured values obtained in the following experimental sets:

- Set 1: resin-bond, M2, medium dress

- Set 2: resin-bond, M2, coarse dress

- Set 3: vitrified-bond, M2, fine dress

- Set 4: resin-bond, ASP2023

- Set 5: vitrified-bond, M2, coarse dress
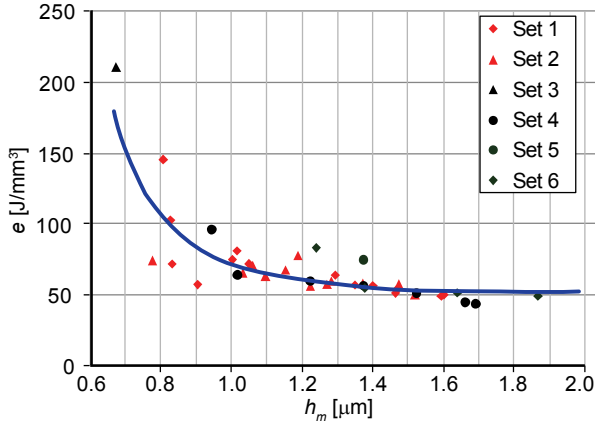
- Set 6: resin-bond, ASP2060

Fig. 2: Specific grinding energy vs. undeformed chip thickness for different experimental sets.

From the same figure it can also be seen that specific grinding energy, e, decreases asymptotically until reaching a minimal steady-state value e_0 of around 50 J/mm^3. In all cases the wheel was dressed relatively sharp. Therefore, we now have a relationship between h_m in the case of a sharp wheel. If we fit a curve to the above data we get the following equation:

$$e = e_0 + \frac{C_2}{h_m^{n_2}} \qquad (3)$$

We have taken the value of specific grinding energy $e = e_0 = 50$ J/mm^3 to be fixed (sharp dress, aggressive cut).

The parameters C_2 and n_2 depend on the dressing and grinding conditions (amount of material removed, wheel wear, grindability, etc.). In this stage of research, the variation of specific grinding energy has not been considered.

4. GEOMETRY AND KINEMATICS

Punch grinding with controlled infeed is accomplished by radially feeding a grinding wheel into the rotating workpiece to produce a punch to a desired geometry, as shown in Figure 3.
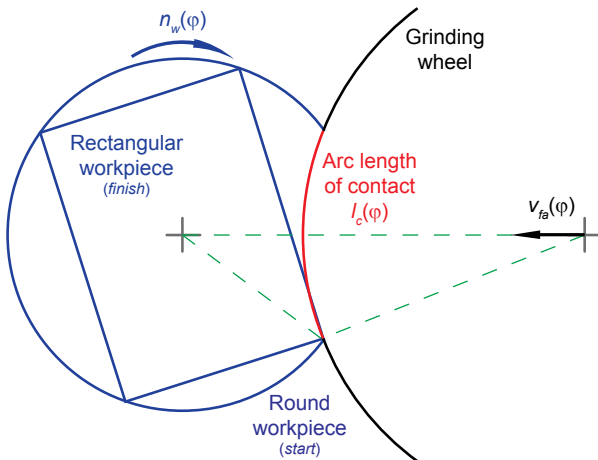

Fig. 3: Illustration of punch grinding operation.

For the needs of modeling the punch-grinding geometry and kinematics, let us consider instantaneous contact conditions at the workpiece rotation angle φ when grinding one side of the workpiece in an i-th grinding pass as shown in Figure 4.

The coordinate system is held fixed on the workpiece. This means that from the simulation point of view the wheel rotates around the workpiece with the relative rotational frequency that equals the actual workpiece rotational frequency $n_w(\varphi)$.
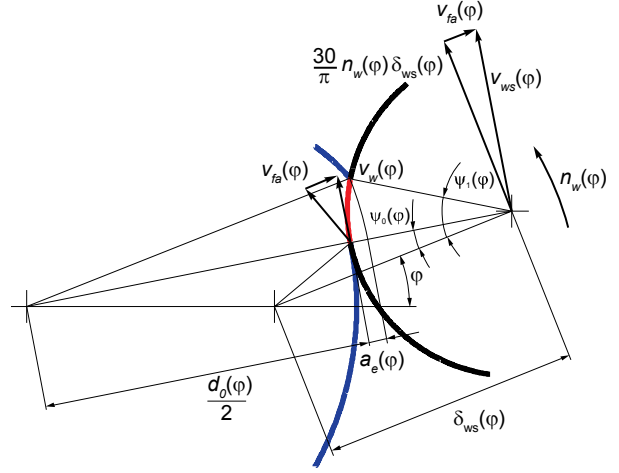

Fig. 4: Punch grinding geometry and kinematics.

Grinding passes (cutting paths) for each side of the workpiece are selected as parts of circles, whose diameters increase from the initial workpiece diameter to infinite value that represents a straight line. The maximum cutting depth, reached in the middle of the side being ground, is the same for all grinding passes.

Penetration area of the grinding wheel into the workpiece results can be characterized by the arc length of the contact $l_c(\varphi)$. Neglecting motions and deformations of the wheel and the workpiece, $l_c(\varphi)$ is calculated as:

$$l_c(\varphi) = \frac{d_s}{2}\left[\psi_1(\varphi) - \psi_0(\varphi)\right] \qquad (4)$$

where d_s is the wheel diameter, $\psi_1(\varphi)$ is the contact entry angle and $\psi_0(\varphi)$ is the contact exit angle.

The instantaneous specific material removal rate $Q'_w(\varphi)$ is calculated as:

$$Q'_w(\varphi) = \left[1 + \frac{a_e(\varphi)}{d_0(\varphi)}\right]a_e(\varphi)v_w(\varphi) \qquad (5)$$

where $a_e(\varphi)$ is the depth of cut, $d_0(\varphi)$ is the diameter of the cutting path and $v_w(\varphi)$ is the relative workpiece velocity given by:

$$v_w(\varphi) = v_{ws}(\varphi) - \frac{15}{\pi}d_s \cdot n_w(\varphi) \qquad (6)$$

where $v_{ws}(\varphi)$ is the relative velocity of the wheel centre:

$$v_{ws}(\varphi) = \frac{30}{\pi} \frac{\delta_{ws}(\varphi)}{\cos \psi_0(\varphi)} n_w(\varphi) \tag{7}$$

and $\delta_{ws}(\varphi)$ is the distance between the workpiece and the wheel centers.

To achieve proper grinding kinematics, the radial infeed velocity $v_{fa}(\varphi)$ should equal:

$$v_{fa}(\varphi) = \delta_{ws}(\varphi) \tan \psi_0(\varphi) \frac{30}{\pi} n_w(\varphi) \tag{8}$$

5. THERMAL MODEL

In the simplified heat-transfer analysis, the maximum grinding temperature rise θ_m is usually calculated by the adapted Jaeger model [11]:

$$\theta_m = \frac{1.13 \cdot q_w}{\sqrt{k \cdot \rho \cdot c_p}} \sqrt{\frac{l_c(\varphi)}{v_w(\varphi)}} \tag{9}$$

where q_w is the heat flux entering the workpiece, l_c is the arc length of contact, k is the thermal conductivity of the workpiece, ρ is the workpiece density, and c_p is the specific heat capacity of the workpiece.

The generation of tensile residual stress is strongly dependant on workpiece properties, in particular material yield stress. The value of the transitional temperature, i.e. the grinding temperature for the onset of tensile residual stress varies from 400 to 600ºC for AISI M2, depending on the heat treatment [3]. For our optimization we are constraining the θ_m to 600ºC, presuming that the likelihood of tensile residual stress generation on the workpiece surface will be minimal.

For calculating θ_m, the parameter which remains to be determined is the heat flux entering the workpiece q_w. Of the total grinding energy, only the fraction, ε known as the energy partition, is conducted as heat to the workpiece at the grinding zone. For a specific grinding energy e or power P (measured using a power meter), the heat flux to the workpiece can be written as:

$$q_w = \frac{\varepsilon \cdot P}{l_c(\varphi) \cdot b} = \frac{\varepsilon \cdot e \cdot Q'_w(\varphi)}{l_c(\varphi)} \tag{10}$$

where b is the grinding width. In the upper equation, the numerator represents the portion of the grinding power entering the workpiece as heat and the denominator is the area of the grinding zone. Both $Q'_w(\varphi)$ and $l_c(\varphi)$ can be predicted by the developed simulation model.

In order to calculate q_w, it is necessary to specify the energy partition to the workpiece ε. The energy partition can be obtained experimentally using temperature matching and inverse heat transfer methods [12]. For shallow cut grinding of steels with aluminum oxide wheels, the energy partition typically varies from about 60 to 85% [13].

6. SIMULATION

Within the simulation model, geometrical mechanism of the workpiece forming and process kinematics are linked-up with the thermal model. The simulation model inputs the following parameters:

- Wheel diameter: 380 mm
- Initial workpiece diameter: 25 mm
- Width and height of the punch: 20 x 15 mm
- Specific grinding energy: 50 J/mm^3
- Energy partition: 60%
- Thermal conductivity of the workpiece: 24 W/mK
- Workpiece density: 8.12 g/cm^3
- Specific heat capacity of the workpiece: 0.46 J/gK

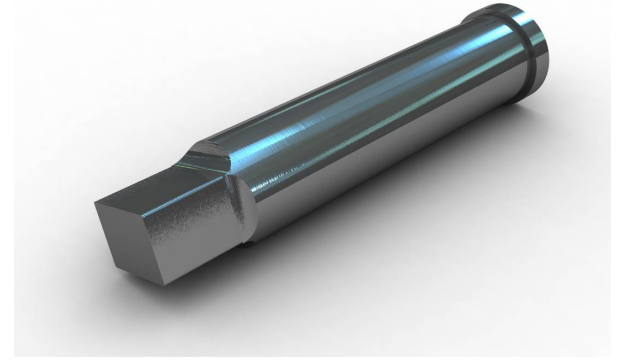The features of the punching tool, used as a case-study for the simulation, are shown in Figure 5.

Fig. 5: Punching tool.

The variations in arc length of contact $l_c(\varphi)$ and specific material removal rate $Q'_w(\varphi)$ are shown in Figure 6 and Figure 7 respectively. Both diagrams are shown for the optimal grinding scenario, consisting of 310 grinding passes (total number of workpiece revolutions). Variations in $l_c(\varphi)$ and $Q'_w(\varphi)$ for the first grinding pass are shown in blue ($i = 1$).
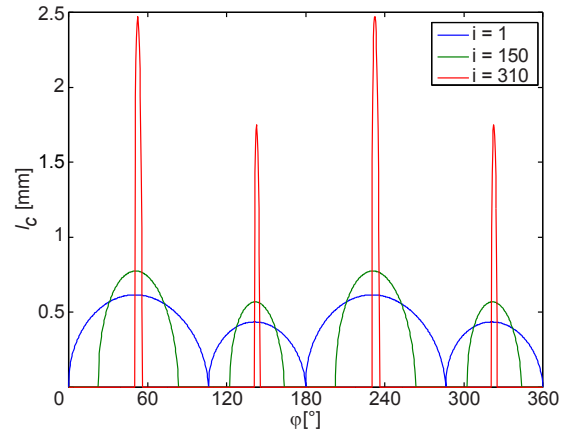

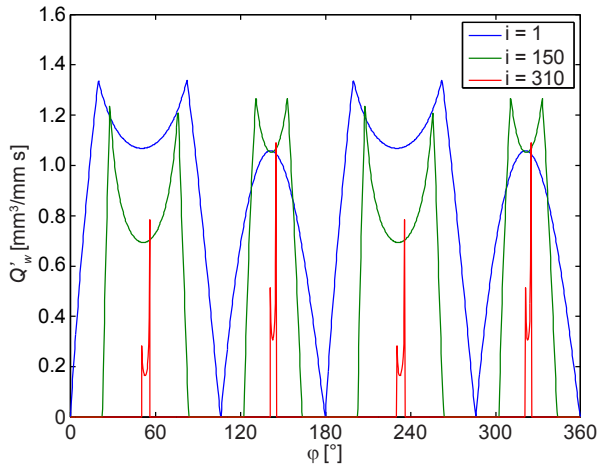**Fig. 6: Arc length of contact vs. angle of workpiece rotation.**

Fig. 7: Specific material removal rate vs. angle of workpiece rotation.

7. OPTIMIZATION

In punch grinding, drastic changes in the grinding conditions occur if the workpiece rotates at constant velocity. The instantaneous specific material removal rate $Q'_w(\varphi)$ can cause localized thermal damage on the punch leading or trailing edge. An approach to overcoming this problem is to vary the workpiece and infeed velocities as to maintain a more constant grinding temperature. In theory, the punch-grinding cycle can consist of a single or multiple passes (number of total workpiece rotations). In the single pass (creep-feed) operation, all material is removed during one rotation of the workpiece. Similarly, punch grinding with multiple passes requires higher workpiece and infeed velocities that are constrained by the workhead speed range and maximal speed as well as acceleration of the cross slide (X-axis). The case study considers grinding on a Studer S33 cylindrical grinding machine, whose major limitation is the maximal infeed (X-axis) of 10 m/min. For this speed, the workpiece rotational frequency is limited to 100 rpm, even though the maximal speed of the workhead is 1500 rpm.

The optimization problem can hence be written as:

- minimize t

- subject to: $T \leq \theta_m$

    $n_w \leq 100$ rpm

    $v_{fr} \leq 10$ m/min

The optimal number of grinding passes that yield minimal grinding cycle time is not known. The optimization problem is solved by the simulation model that yields optimal number of grinding passes and grinding parameters satisfying the optimization objective and constraints. Considering the wheel speed is fixed, only the workpiece and infeed velocities are to be optimized. The major output of the optimization is $n_w(\varphi)$, shown in Figure 8.
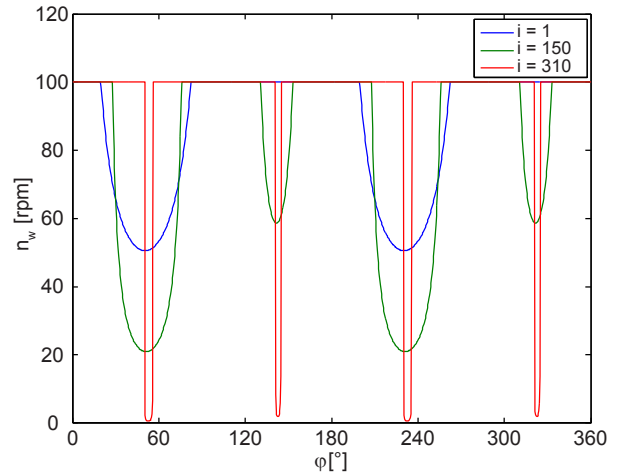

Fig. 8: Variation of workpiece rotational frequency.

We can see from the upper figure that the workpiece velocities, or $n_w(\varphi)$, are increasing during successive grinding passes. The upper limit of worpiece velocity is achieved in the last grinding pass. In the optimal scenario, consisting of 310 grinding passes, the minimal grinding cycle time of t = 6.4 minutes is achieved. Grinding cycle time depends on the number of required grinding passes N, i.e. the total number of workpiece revolutions. As we see in Figure 9, the minimal grinding cycle time is achieved when N=310. Grinding in one pass (creep-feed) scenario would be far from optimal, resulting in the cycle time of t = 85.3 minutes.
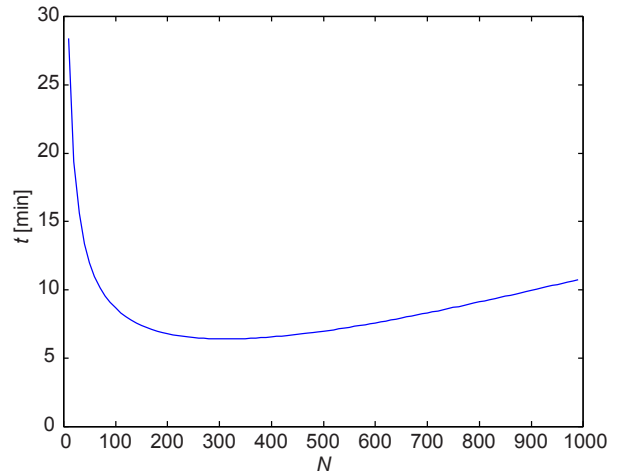

Fig. 9: Grinding cycle time vs. number of grinding passes.

8. CONCLUSIONS

The idea of this paper is to present an overview and particularities of punch grinding operation and to discuss analytical approaches to simulate thermal behavior, geometry and kinematics of the process. Simulation model, incorporating all three aspects, is used to optimize the process so that the grinding cycle time is minimized.

Tensile residual stress is one of the main limitations of a punching tool, so it is especially important to avoid their generation. This can be achieved by constraining maximum grinding zone temperature rise. A critical factor needed for calculating this temperature and controlling the onset of tensile residual stress is the specific grinding energy and the energy partition. More experimental work is required to adequately estimate the energy partition and to account for specific energy variation with dressing and grinding conditions. Experiments are currently being conducted, with measurements of specific grinding energy, depth of thermal damage (i.e. rehardening burn and thermal softening). These measurements will enable the calibration of the simulation model.

While this thermal analysis is currently being developed further, the simplified model presented here is sufficient to give relative temperature values, enabling the model to determine parameters that give minimal cycle time.

It is clear, however, that the specific energy and its partition to the workpiece should be kept low. One way to achieve this is to have sufficient self-sharpening of the wheel that reduces the specific grinding energy. Another way to achieve cooler grinding would be to use CBN wheels, which have higher thermal conductivity (carrying more heat away from the grinding zone than aluminium-oxide wheels). Last but not least, cooling efficiency must be separately optimized to take maximal amount of heat by the grinding fluid and to further lower the energy partition.

9. ACKNOWLEDGEMENTS

10. REFERENCES

[1] Snoeys, R., Maris, M. and Peters, J. (1978), Thermally induced damage in grinding, *CIRP Annals - Manufacturing Technology*, **27/2**, 571-581.

[2] Meurling, F., Melander, A., Tidesten M. and Westin, L. (2001), Influence of carbide and inclusion contents on the fatigue properties of high speed steels and tool steels, *International Journal of Fatigue*, **23**, 215-224.

[3] Chen, X., Rowe, W. B. and McCormack, D. F. (2000), Analysis of the transitional temperature for tensile residual stress in grinding, *Journal of Materials Processing Technology*, **107**, 216-221.

[4] Baliga, B., Doyle, E. D. and Thompson, W. (1998), Computer simulation for punch grinding, *Transactions of Mechanical Engineering*, **23/1**, 9-17.

[5] Baliga, B., Hodgson, P. and Doyle, D. (1999), Effect of contact length in off-round grinding, In: *Abrasive Technology: Current Development and Applications I* (Jun Wang. (Ed.)), 116-123. World Scientific Publishing, Singapore.

[6] Malkin, S. and Guo, C. (2008). *Grinding technology: Theory and applications of machining with abrasives*. Industrial Press, New York.

[7] Badger, J. A. (2007). Grindability of conventionally produced and powder-metallurgy high-speed steel, *CIRP Annals - Manufacturing Technology*, **56/1**, 353-356.

[8] Rowe, W. B. (2009). *Principles of modern grinding technology*. William Andrew Publishing, Norwich.

[9] Shaw, M. C. (1996). *Principles of abrasive processing*, Oxford University Press, Oxford.

[10] Badger, J. A. (1999), A computer model to predict grinding forces from abrasive wheel topography, *Ph.D. Thesis*, Trinity College, Dublin.

[11] Jaeger, J. C. (1942), Moving sources of heat and the temperature at sliding contacts, *Proceedings of the Royal Society of New South Wales,* **76**, 203-224.

[12] Malkin, S., Guo, C. (2007), Thermal analysis of grinding, *CIRP Annals - Manufacturing Technology*, **56/2**, 760-782.

[13] Kohli, S., Guo, C., Malkin, S. (1993), Energy partition to the workpiece for grinding with aluminum oxide and CBN abrasive wheels, *ASME Journal of Engineering for Industry*, **117**, 160-168.